REVIEW

doi:10.1038/nature12608

Sound and heat revolutions in phononics

Martin Maldovan[1,2]

The phonon is the physical particle representing mechanical vibration and is responsible for the transmission of everyday sound and heat. Understanding and controlling the phononic properties of materials provides opportunities to thermally insulate buildings, reduce environmental noise, transform waste heat into electricity and develop earthquake protection. Here I review recent progress and the development of new ideas and devices that make use of phononic properties to control both sound and heat. Advances in sonic and thermal diodes, optomechanical crystals, acoustic and thermal cloaking, hypersonic phononic crystals, thermoelectrics, and thermocrystals herald the next technological revolution in phononics.

In recent decades, major technological revolutions have transformed our society and daily lives. Their remarkable innovations have been based primarily on our improved ability to manipulate two particles: electrons and photons. In particular, the control of electrons in semiconductor materials has generated fundamental changes, with laptops, mobile telephones and digital cameras now products that seem always to have existed. Analogously, the development of materials and devices with which to control photons has generated major changes in society, such as wireless communication and the use of optical fibres and microwaves. The successful management of the electromagnetic spectrum is demonstrated by the wide range of frequencies controlled in electromagnetic devices, which extends over 14 orders of magnitude, ranging from positron emission tomography (PET) scanning at frequency $f \approx 10^{20}$ Hz to amplitude-modulation (AM) radios at $f \approx 10^{6}$ Hz.

Besides electrons and photons, another everyday particle is the phonon, which is responsible for the transmission of sound and heat. Given the many applications of our remarkable success in managing electrons and photons, it would be valuable to achieve a similar degree of control over the particle that accounts for both sound and heat (Fig. 1). Although some sonic and thermal devices and materials, such as medical ultrasound imaging machines and thermal insulation materials, are well known, further applications for phononic devices are developing fast, from thin acoustic metamaterials that can soundproof rooms to enhanced thermoelectric devices that can use our bodies' waste heat to power portable electronic devices.

In this review, I provide insights on newly developed phononic materials and devices that have recently been shown to have remarkable physical properties—making it possible to manipulate sound and heat with unprecedented precision. I begin with a classical description of small-scale phononic crystals, followed by recent progress on unidirectional sound transmission in acoustic diodes—analogous to electronic diodes—and new developments on acoustic cloaking using metamaterials. I examine novel interactions between sound and light in resonant cavities, and discuss new advances in thermal diodes and thermal metamaterials. I also provide an overview on thermoelectric materials (which convert heat into electricity) and discuss novel thermocrystals, which treat heat like sound and bring phonon management to the boundary zone between sound and heat. These recent ideas and concepts have improved our ability to manage the phononic spectrum, providing exciting opportunities to develop a large variety of devices that can control sound and heat.

Hypersound and heat control by phononic crystals

Sound and heat can both be described as mechanical vibrations transmitted through the atomic lattice. One difference between them, however, is that most sound waves oscillate at low frequencies (kilohertz) and propagate over large distances, whereas most heat vibrations oscillate at high frequencies (terahertz) and travel small distances. These different features lead scientists and engineers to employ different strategies to control sound and heat propagation. Essentially, macroscale and microstructured materials are able to manipulate sound and hypersound (very high-frequency sound, with $f \approx 1$ GHz) frequencies, whereas to control heat, nanostructures are generally required. The development of sonic and thermal devices thus requires the design, fabrication and characterization of composite materials ranging from the centimetre scale to the nanometre scale.

Over the past two decades, the propagation of sound waves with frequencies in the range from kilohertz to megahertz has been efficiently controlled by phononic crystals—artificial periodic structures made of two elastic materials[1,2] (Fig. 2). Although these structures were initially designed to control sound, in recent years small-scale phononic crystals have been successfully used to control hypersound and heat. In phononic crystals, mechanical waves with frequencies within a specific range are not allowed to propagate within the periodic structure. This forbidden frequency range—the 'phononic bandgap' (PBG)—allows sound to

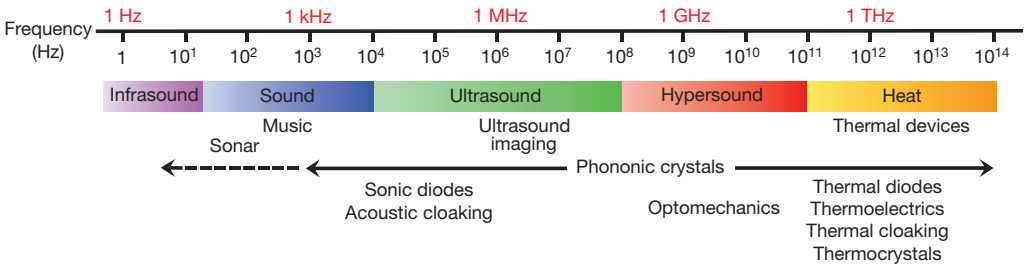

Figure 1 | The phononic spectrum.

[1]Department of Materials Science and Engineering, Massachusetts Institute of Technology, 77 Massachusetts Avenue, Cambridge, Massachusetts 02139, USA. [2]School of Chemical and Biomolecular Engineering, Georgia Institute of Technology, North Avenue, Atlanta, Georgia 30332, USA.

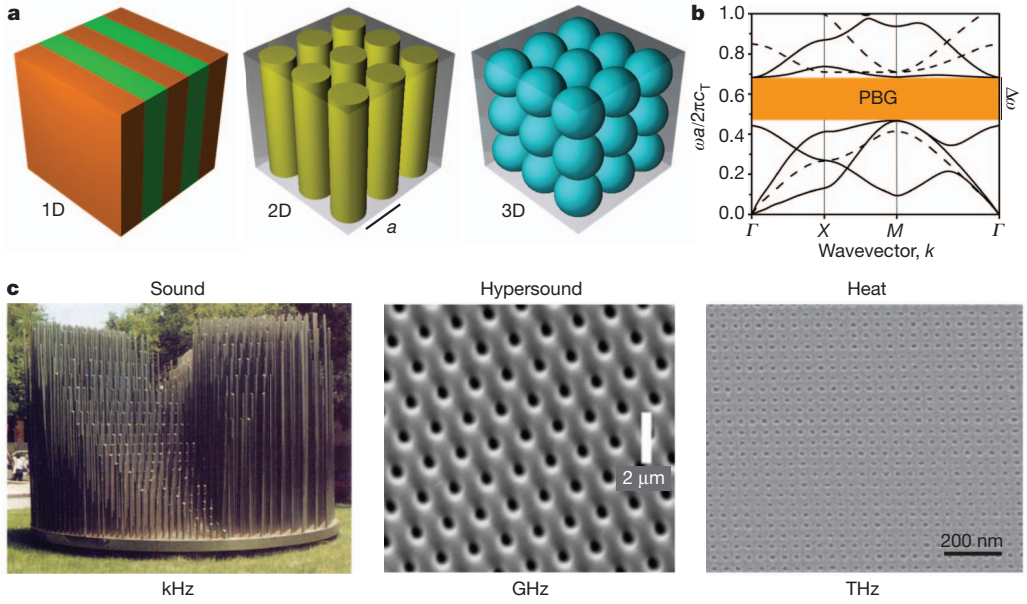

Figure 2 | Phononic crystals. **a**, 1D, 2D and 3D phononic crystals made of two different elastic materials arranged periodically. Different colours represent materials with different elastic properties. **b**, An example of a phononic band diagram $\omega = \omega(k)$ for a two-dimensional phononic crystal, in which non-dimensional frequencies $\omega a/2\pi c_T$ (with c_T a transverse velocity) are plotted versus the wavevector k along the Γ–X–M–Γ path in the square Brillouin zone. The range of forbidden frequencies, or PBG, is shown in orange. **c**, 2D phononic crystals with periodicities a in the centimetre range (left), the micrometre range (middle) and the tens-of-nanometres range (right) can be used to control sound, hypersound and heat, respectively. Images are taken from fig. 1 of ref. 3 (left image, with permission), fig. 1a of ref. 8 (middle image) and fig. 1b of ref. 11 (right image, with permission).

be controlled in many useful ways in structures that can act as sonic filters, isolators, waveguides or resonant cavities. Owing to wave interference effects, PBGs occur for phonon wavelengths λ that are comparable to the structure periodicity a (Fig. 2). For experimental convenience, a large number of phononic crystals have been fabricated at macroscopic scales ($a \approx 10$ cm–1 mm) to control sound of frequency $f \approx 10^3$ Hz and ultrasound of $f \approx 10^6$ Hz (refs 3–7), finding promising applications in acoustics, medical diagnosis and remote sensing. In recent years, however, the challenge has been to fabricate phononic crystals having small periodicities $a < 1$ μm, to control high-frequency ($f \approx 10^9$–10^{12} Hz) phonons[8–11]. Given that the periodicity of small-scale ($a \approx 1$ μm) phononic crystals can be comparable to the wavelengths of light, these crystals can provide bandgaps for both hypersound and light, suggesting new mechanisms with which to enhance phonon–photon interactions[12]. By additionally reducing the periodicity to the nanometre scale, the applications of small-scale phononic crystals can be extended from sound to heat, because PBGs could in principle exist in the terahertz regime. As shown later, however, this reasoning requires a more precise analysis owing to the different characteristics of sound and heat transfer.

A small-scale phononic crystal for hypersound frequencies $f \approx 1$ GHz has been fabricated using interference lithography[8]. This technique provides single-crystalline periodic structures by transferring a laser intensity pattern into a photosensitive material. The phononic crystal consists of a triangular array of air holes in an epoxy matrix, with lattice periodicity $a = 1.36$ μm (Fig. 2c). To characterize the phonon modes, Brillouin light scattering is employed, which provides complete phononic band diagrams for the dispersion relation for phonon modes propagating within the crystal (Fig. 2). Other small-scale phononic crystals were constructed by self-assembling single-crystalline colloidal films of polystyrene spheres into a face-centred-cubic lattice[9]. The small size of the spheres used ($d = 256$ nm) guarantees operation in the hypersonic frequency range. By employing Brillouin light scattering to map the dispersion relation of longitudinal phonons, a hypersonic (gigahertz frequency) PBG was measured. The significance of these small-scale architectures is that, in addition to providing simultaneous gaps for hypersound and light, they greatly extend the use of phononic crystals from sonic and ultrasonic frequencies to the hypersonic regime[8–10]. This increases the range of phononic frequencies that can be controlled by three orders of magnitude.

More recently, a state-of-the-art nanometre-scale phononic crystal was fabricated by transferring the patterns of two intersecting arrays of platinum nanowires into a silicon epilayer (Fig. 2c)[11]. The phononic 'nanomesh' consists of a square-lattice silicon matrix of air holes, with $a = 34$ nm. The key feature of this structure is that it reduces the thermal conductivity of bulk silicon by almost two orders of magnitude. Heat in silicon is mostly carried by phonons with 10^{12} Hz frequencies, so this demonstrates that reducing the size of phononic crystals to the nanometre scale can modify and control the propagation of high-frequency phonons, extending the applications of phononic crystals from sound to heat[11]. As I explain below, however, the mechanism behind the reduction of the thermal conductivity is not based on coherent interference and PBGs—as in classical phononic crystals—but is mainly due to the diffuse scattering of phonons at interfaces.

With the recent progress in synthesis and characterization of small-scale materials, it is now possible to fabricate phononic crystals with periodicities ranging from centimetres to nanometres[3–11]. These advances have significantly increased the ability to manage the phonon spectrum, where the frequencies that can now be controlled extend from 10^3 Hz to 10^{12} Hz, a range of nine orders of magnitude. As I show in this review, the wide range of control over phonon frequencies—comparable to the wide range of control over electromagnetic frequencies—allows the realization of many exciting devices that can manipulate phonons at all relevant frequencies: sound, ultrasound, hypersound and heat.

Acoustic diodes

In electronics, a diode is a well-known device that allows electrical current to pass in one direction but not in the opposite direction. This fundamental principle—which led to a revolution in electronics—has recently been demonstrated for sound waves[13–15]. The development of the acoustic counterpart of the electronic diode opens up exciting opportunities for novel applications in different research areas ranging from biomedical ultrasound imaging to environmental noise reduction.

A sonic diode showing unidirectional transmission was constructed using a one-dimensional (1D) phononic crystal made of alternating layers of glass and water coupled to a nonlinear acoustic medium[13,14] (Fig. 3a). A sound wave incident from the left, with frequency ω inside the PBG, is partially converted within the nonlinear medium to a secondary wave with frequency 2ω. Because ω lies in the PBG, the original wave is reflected backwards, but the secondary wave with frequency 2ω outside the PBG can freely pass through the structure (Fig. 3a). On the other hand, if the sound wave is incident from the right, the wave is completely reflected in the backward direction because ω lies inside the PBG. As a result, a sound wave with frequency ω can pass through the

system only along the forward direction, providing unidirectional sound transmission. In experiments[14], the layers were about 1 mm thick, allowing the diode to operate at ultrasound frequencies in the megahertz range.

An even more interesting approach using linear materials has been introduced by means of a two-dimensional (2D) phononic crystal made of a square lattice of steel rods in contact with a diffraction structure[16] (Fig. 3b). The critical feature in this diode is that one of the external surfaces is 'smooth' while the other is 'rough'. Waves incident on the smooth surface (reverse direction) with frequencies ω inside the PBG ($\sim$10 kHz) are reflected backwards because they fall into the forbidden frequency range. In contrast, waves incident on the rough surface (forward direction) can pass through partially. Because the outgoing waves in the forward direction are not parallel to the incident waves, the acoustic energy is converted through high-order diffractions to other modes with different spatial frequencies to overcome the barrier imposed by the PBG[16]. The main advantage of the linear acoustic diode is that sound waves do not change their frequencies as they pass through the structure. Also, its easy fabrication method opens up opportunities for on-chip planar acoustic circuits with applications in logical sound processing.

Sound rectification has also been demonstrated in 1D granular crystals[17] consisting of a chain of steel spheres interacting nonlinearly (Fig. 3c). This system allows wave propagation for frequencies lower than a certain cut-off ω_C. When a defect sphere is added, a localized mode with frequency $\omega_D > \omega_C$ is created around the defect. An incident wave with $\omega > \omega_C$, and below ω_D, along the reverse direction (right to left) cannot propagate through the crystal because of the PBG. However, if moving along the forward direction (left to right), a wave with frequency ω—having low amplitude—does not pass through but excites the vibrational mode localized around the defect sphere. If the wave's amplitude is increased, its acoustic energy is converted to modes with frequencies outside the gap ($\omega < \omega_C$) that can freely pass through the structure, generating unidirectional transmission.

The experimental realizations of acoustic diodes, providing unidirectional sound transmission, are major steps towards complex acoustic devices that could greatly increase the efficiency of ultrasound medical systems, non-destructive testing and environmental noise control. Like its electric counterpart, the sonic diode may produce unexpected consequences, in acoustics rather than electronics.

Acoustic invisibility cloaks by metamaterials

Another exciting and novel opportunity to control sound waves involves the design and fabrication of acoustic cloaking shells. The basic idea is to use a shell to guide acoustic waves around a certain object such that the object inside the shell becomes 'invisible' (undetectable by sound waves) (Fig. 4a). Although cloaking devices were initially introduced for electromagnetic waves[18,19], these principles have recently been extended to sound waves[20–33]. Essentially, to obtain a cloaking device for acoustic waves, the cloaking shell surrounding the object must be made of an engineered artificial material, known as acoustic metamaterial, in which elastic properties such as mass density and bulk modulus are anisotropic and spatially dependent.

An acoustic cloaking shell was introduced by considering the similarity between the 2D electromagnetic and acoustic wave equations[21]. The cylindrical shell is made of a metamaterial fluid with inhomogeneous bulk modulus and an anisotropic and inhomogeneous mass density that redirects pressure waves around the object (Fig. 4a). Cloaking effects have been extended to three dimensions by noting the isomorphism between the acoustic wave equation and the electrical conductivity equation[22]. Such three-dimensional (3D) cloaks are also obtained by considering zero scattering effects in the acoustic wave equation[23]. Because the 2D and 3D cloaking shells require complex materials, it is challenging to implement such metamaterials in experiments. Owing to this difficulty, additional theoretical approaches have been developed in which layered cylindrical cloaking shells are considered to obtain the required values for mass density and bulk modulus[24–26].

To overcome the difficulty associated with material requirements, an innovative approach based on the analogy between acoustic elements and electronic circuits has been employed to design and fabricate a 2D cylindrical cloak (Fig. 4b)[27,28]. The basic idea is to convert the acoustic material to an analogous network of inductors L and capacitors C, where

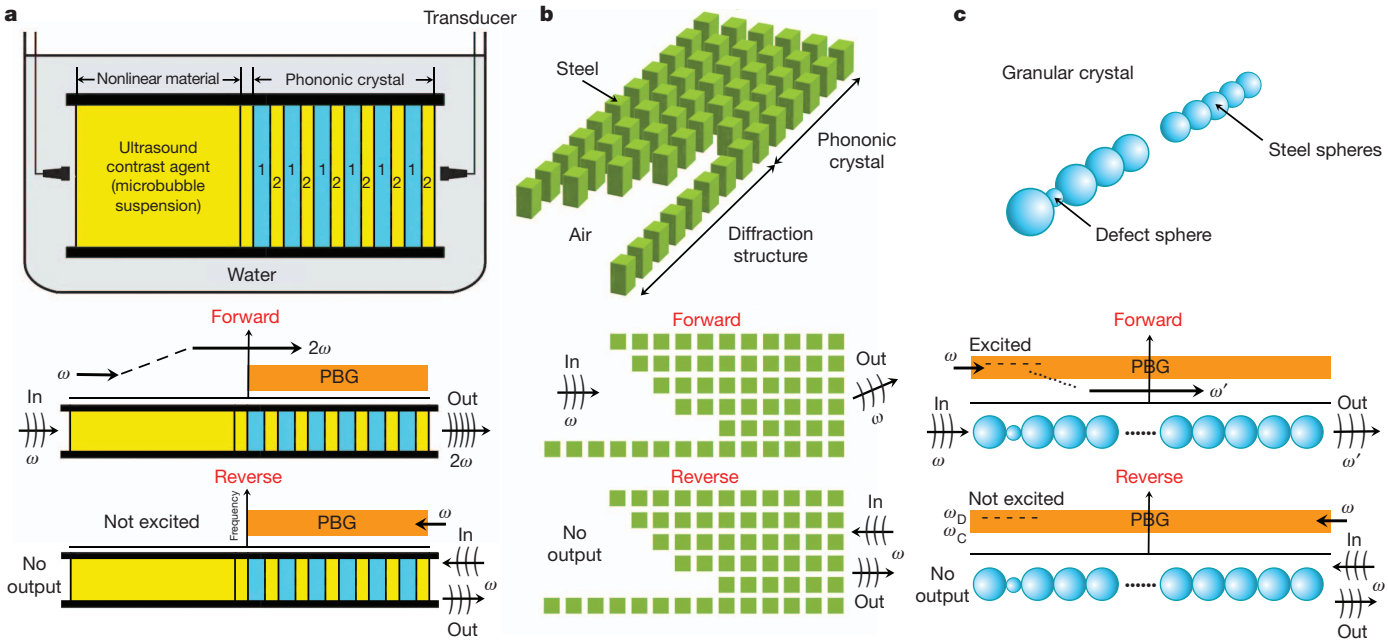

Figure 3 | Acoustic diodes. **a**, An acoustic diode made of a 1D phononic crystal (alternating layers of glass and water) coupled to a nonlinear acoustic medium[14]. A sound wave with frequency ω within the PBG can evade the PBG—and pass through the system—only from left to right (forward direction), owing to the change of frequency $\omega \rightarrow 2\omega$ in the nonlinear medium. **b**, A linear acoustic diode consisting of a 2D phononic crystal (square steel rods with $d = 4$ mm in a square lattice with $a = 7$ mm) and a diffraction structure[16]. Waves with frequency ω within the PBG cannot pass through the structure if they are incident on the phononic crystal (reverse direction), but they can propagate if they are incident on the diffraction structure (forward direction). **c**, Sound rectification in 1D granular crystals (steel spheres with radius 9.53 mm and mass 28.84 g)[17]. A defect sphere creates sound rectification by introducing localized states with frequencies ω_D that allow incident waves to evade the PBG (and pass through) by changing frequencies from ω to ω' (forward direction).

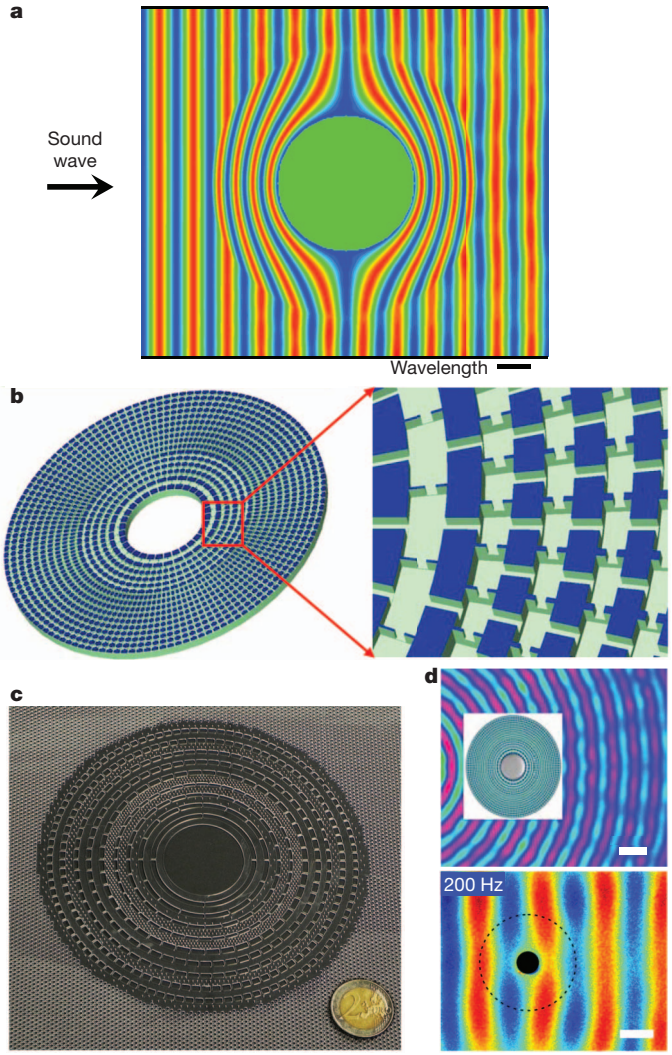

Figure 4 | Acoustic cloaking. **a**, A sound wave incident on a rigid cylinder surrounded by a cloaking shell. The wave passes through the shell and propagates as it would have done in the absence of an obstacle. Reproduced from fig. 2 of ref. 25 with permission. **b**, A cylindrical acoustic cloak for ultrasound waves in water. Reproduced from fig. 2a of ref. 27 with permission. **c**, Cloaking shell for elastic waves made of concentric cylinders of PVC and PDMS. The coin diameter is 25.75 mm. Reproduced from fig. 2 of ref. 31 with permission. **d**, The measured pressure from a 60-kHz point source for a steel cylinder (grey) surrounded by the cloaking shell (light-blue coating around the cylinder) from **b**, where waves pass largely unperturbed (top). Scale bar, 2.7 cm. Elastic waves propagating through a cylinder (black) with the cloaking shell (dotted circular line) from **c**. The shell avoids disruption of the elastic waves (bottom). Scale bar, 5 cm. Reproduced from figs 3d and 3b of refs 27 and 31 with permission.

the motion of the fluid is equivalent to the electrical current, and the mass density and bulk modulus are related to the capacitance C and inductance L. Using this 'transmission line' approach, an aluminium plate having an array of cavities (acting as acoustic capacitors) connected by channels (acting as acoustic inductors) was designed to perform as an acoustic cloak for ultrasound waves (Fig. 4b). The aluminium-based cloak was placed in a water tank (with an object within the shell) to compare ultrasound waves around the object with and without the cloak. When the object is surrounded by the metamaterial cloak, the incoming wave is restored behind the object with very little distortion, making the cloak and the object 'invisible' to ultrasound waves in water[27]. This acoustic cloak—fabricated in the millimetre length scale—operates over a wide range of ultrasound frequencies (40–80 kHz). A previous cloak, fabricated at the centimetre scale, but designed for surface waves in a liquid material, has also provided cloaking effects in the range of 10-Hz frequencies[29].

Besides full cloaks in water, an acoustic cloak that works in air, and for audible frequencies 1–4 kHz, has been designed, fabricated and characterized using acoustic metamaterials[30]. This cloak, however, is based on a different technique known as 'ground cloaking', because the object to be made 'invisible' is located on a reflecting surface. The object on the surface is covered with a coating whose metamaterial properties are given by coordinate transformation acoustic theory. The function of the coating is to make the object invisible. The metamaterial coating is made of a stack of planar perforated plastic plates, in which the size (millimetres) and shapes of the perforations are used to design the acoustic properties for cloaking. Using a 3-kHz speaker as a sound source, it is shown that the reflected acoustic field from the ground surface alone and that from the ground surface and the coated object are essentially identical, thus demonstrating a new way of cloaking objects from sound waves in air[30].

A cloaking shell for elastic waves[31], fabricated using a structured polymer plate, demonstrates that theory and experiments on acoustic cloaking can be expanded from fluids to solid materials (Fig. 4c)[31–33]. The solid cloaking shell consists of 20 concentric rings, each a tailored composite of polyvinyl chloride (PVC) and polydimethylsiloxane (PDMS) that allowed the Young's modulus within the shell to be specified and cloaking effects to be obtained. To show the cloak in operation, elastic sound waves were guided through the shell (and around the object to be concealed) and their movement was recorded using a stroboscopic imaging technique. For frequencies of 200–400 Hz, the elastic waves can pass through the cloaking shell and propagate as they would have done without an obstacle—thus demonstrating acoustic cloaking in solid materials (Fig. 4d). This cloak is based on a theoretical proposal that modifies the technique of coordinate transformation of Maxwell's equations to create cloaking shells for elastic flexural waves in solids[32]. Recently, a theoretical approach for the control of coupled pressure and shear waves in elastic solids has also been introduced[33].

The remarkable progress made in recent years in acoustic cloaking is evident from the large number of devices designed to hide objects from sound waves, which include air, water and solid-material platforms. In analogy with their electromagnetic counterpart, acoustic cloaking and metamaterials open up new ways to manipulate sound. Such metamaterials can be used to soundproof studios and buildings, design concert halls, control environmental noise, make ships invisible to sonar waves, or even design shields against seismic waves. Metamaterial concepts and devices bring together different research areas, including cosmology, physics, materials science and civil engineering.

Enhancing the interaction between sound and light

Interaction between phonons and photons is well known in studies of Raman spectroscopy and Brillouin scattering processes. Recently, a mechanism involving the simultaneous localization of mechanical and optical waves by using acoustic and optical cavities has been introduced greatly to enhance sound and light interactions. This raises the prospect of a new class of acousto-optical crystal that can integrate the combined management of phonons and photons[12,34–59].

A 1D crystal showing simultaneous localization of sound and light by resonant cavities was introduced by constructing an acoustic cavity within another optical cavity[34,35] (Fig. 5a). The optical cavity is made of $Al_xGa_{1-x}As$ and AlAs layers grown by molecular beam epitaxy, within which a spatially localized optical mode (red) can be created by introducing a defect layer. Similarly, the acoustic cavity is constructed by GaAs and AlAs layers, with a defect $Al_xGa_{1-x}As$ layer that localizes sound modes (blue). The key feature of the system is that, owing to their relatively large wavelengths, photons see the acoustic layered structure as a homogeneous defect layer. In particular, when an incident laser photon excites the localized mode in the optical cavity, this mode splits photoelastically into a localized phonon mode in the acoustic cavity and a localized Stokes mode in the optical cavity. These localized phonons and photons leave the cavities by tunnelling through the layers. Measurements of the light spectrum for the outgoing photons clearly show the energy shift caused by these novel confined acousto-optical interactions[34,35].

A different approach, in which sound and light are both localized in the same cavity, considered the use of periodic structures acting as both phononic and photonic crystals (Fig. 5b)[12]. In analogy to phononic crystals, periodic dielectric structures such as photonic crystals can precisely control light propagation[36–39]. An effective mechanism with which to create non-propagating localized states is the introduction of a defect in a periodic structure having a frequency bandgap[38,39]. Although extensive work has been focused on separate architectures for phononics and photonics, the existence of a PBG does not imply that the structure has a photonic bandgap and vice versa. These dual-bandgap (or 'deaf and blind') structures have been demonstrated by considering an array of air cylinders in a silicon matrix (Fig. 5b)[12,39]. By taking advantage of simultaneous gaps, a defect is introduced to create a single cavity that localizes both phonons and photons. In particular, it was indicated that if the structure periodicity is $a \approx 150$ nm, the cavity can co-localize 500-THz photons and 20-GHz phonons[12]. The simultaneous confinement of phonons and photons in a single cavity is suggested greatly to increase acousto-optical interactions, leading to a different class of planar acousto-optical devices that can integrate both light and sound management[12].

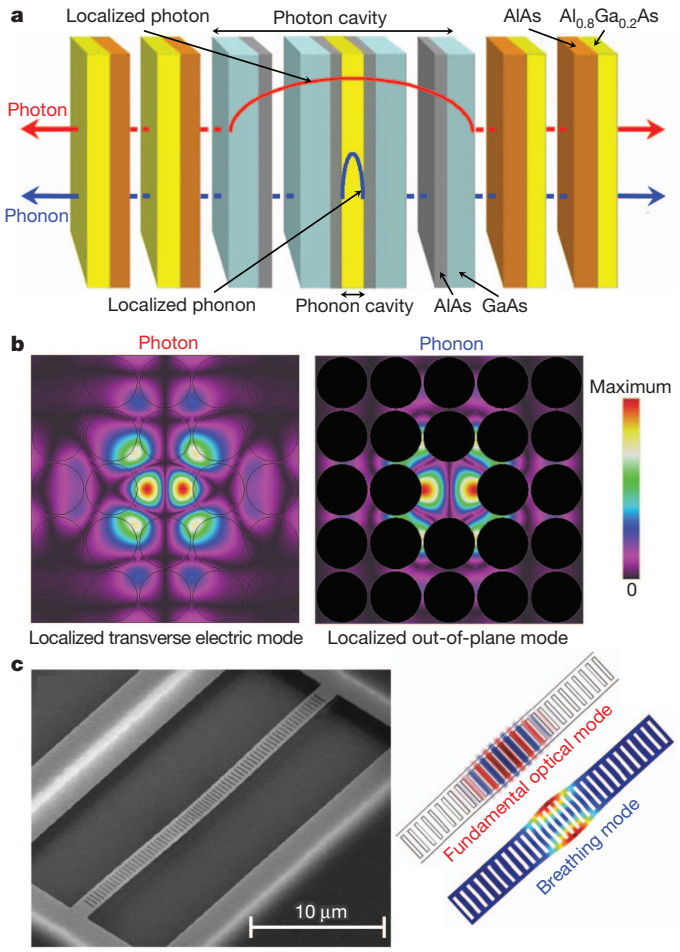

Figure 5 | Enhancing sound–light interaction. **a**, An array of semiconductor layers creates an acoustic cavity within an optical cavity. A light beam entering the structure excites a localized light mode (red) within the optical cavity and a localized sound mode (blue) within the acoustic cavity. Light and sound escape by tunnelling—allowing their interaction to be measured. **b**, Periodic structures having dual photonic–phononic bandgaps can localize both sound and light in the same cavity. Transverse electric (TE) photons are localized within a structure made of air cylinders in silicon by creating a cavity (the missing cylinder) (left). Out-of-plane phonons are localized in the same dual photonic–phononic cavity (right). Co-localization can greatly enhance acousto-optical interactions. Images taken from fig. 3 of ref. 12. **c**, Co-localization and interaction of photons and phonons in a nanobeam with a central defect. Scanning electron microscope image for the nanobeam device (left). Optical and mechanical field distributions for co-localized and coupled opto-mechanical modes (right). Reproduced from figs 1 and 2a of ref. 40 with permission.

More recently, co-localization and interaction of 200-THz photons and 2-GHz phonons has been demonstrated[40] by the design, fabrication and characterization of a 1D silicon nanobeam with rectangular air holes (Fig. 5c). To co-localize optical and mechanical modes at the centre of the structure, a 'defect' is introduced by quadratically—and symmetrically—decreasing the periodicity from the nanobeam centre. Electric and mechanical field distributions for co-localized optical and mechanical modes are shown in Fig. 5c. In this system, the optical modes are excited by using a tapered optical fibre that also collects the transmitted light. Mechanical modes that can couple to optical modes are classified (according to their increasing frequencies) as 'pinch', 'accordion' and 'breathing'. By measuring their radio-frequency spectrum, the character of these modes is described by evaluating the phase and amplitude change of the transmitted light. Importantly, the demonstration of phonon–photon coupling in a planar 'optomechanical' crystal allows for new methods of probing, stimulating, and using mechanical and optical interactions on a chip-scale platform[40].

The prospects of manipulating sound and light by co-localization in periodic crystals have stimulated significant research in recent years. This includes 1D vertical-cavity crystals[41,42], 2D and quasi-2D planar crystals[43–53] and 3D crystals[54,55], involving exciting phenomena such as phoxonic gaps, optomechanical coupling, laser cooling, light modulation, quantum motion and phonon laser action[41–55]. In addition, acousto-optical studies on crystal fibres (which have a solid silica central core surrounded by a lattice of hollow channels extending axially along its length) show interesting phenomena caused by the strong confinement of light and acoustic vibrations[56–59]. These effects include multi-peak Brillouin spectra with frequency shifts in the 10-GHz range, as well as Raman-like nonlinear forward scattering of light with gigahertz phonons[58,59]. These results show that separate research areas such as those involving sound control in phononic crystals and light management in photonic crystals can be successfully merged into a field of dual phononic–photonic crystal materials.

Thermal diodes

The experimental realization of materials and devices that can provide unidirectional transmission of heat is more difficult than in the case of acoustic diodes. This is because heat is carried by a broad spectrum of high-frequency (terahertz) phonons, which are difficult to control. Despite this, novel theoretical and experimental concepts have been introduced whereby heat can flow only in a particular direction[60]. A theoretical thermal diode was proposed by means of two coupled one-dimensional lattices with particles interacting with each other through nonlinear sinusoidal potentials (Fig. 6a). In the forward direction ($T_L > T_R$), the broad spectrum of one chain overlaps with that of the other chain, allowing heat to flow through the structure. In the reverse direction ($T_L < T_R$), however, the vibrational frequencies of the lattices do not match and heat cannot flow through. This match–mismatch of the vibrational modes gives rise to the unidirectional transmission of thermal energy. Thermal rectification effects are achieved by carefully considering different strengths in the potentials of the two segments of the lattice[60]. This theoretical model is a simplified version of a previously proposed diode involving a three-segment 1D nonlinear chain[61]. In recent years, the thermal diode concept has been expanded to include the thermal counterparts of the components of digital electronic circuits—the thermal transistor and thermal logic gates[62,63]. However, important material challenges must still be overcome before their practical realization and use as thermal devices.

In experiments, thermal diodes were fabricated using carbon nanotubes and boron nitride nanotubes[64]. To investigate asymmetric thermal motion, amorphous $C_9H_{16}Pt$ is deposited non-uniformly along the length of the tubes (Fig. 6b). When the heat flows from the high-mass region (left) to the low-mass region (right), the measured thermal conductance is higher. Specifically, for carbon nanotubes and boron nitride nanotubes respectively, the conductance along the nanotube axis is 2%

and 7% larger than that in the reverse direction. To interpret these results, it was suggested that boron nitride nanotubes show larger thermal rectification effects owing to their strong ionic bonds, which favour nonlinear effects. This mechanism has subsequently been theoretically described by considering a 1D anharmonic lattice with a mass gradient. In agreement with experiments, this system provides a larger flow of heat when the heavy-mass end is set at a higher temperature[65]. The major impact of the electrical diode in electronic circuits suggests that highly efficient thermal diodes could have a similar influence in a large number of systems that require precise heat control, such as nanoelectronic devices and energy-saving buildings.

Thermal metamaterials and heat cloaking

Another interesting idea is to apply the metamaterial methods that are used for sound manipulation to the management of heat conduction. This concept has recently been proposed by realizing that mathematical techniques to transform Maxwell's equations[18,19] can be adapted to the Fourier heat equation[66–70]. Controlling heat conduction has always been a difficult scientific challenge. Using newly designed thermal metamaterials[66–70], however, several striking effects on diffusive heat transfer have been implemented, offering a new way to manipulate heat flow (Fig. 7).

Thermal metamaterials were introduced by considering a cylindrical shell that, under a thermal gradient, maintains the inner region at constant temperature, that is, the core is 'invisible' to the thermal gradient[19,66]. Interestingly, it was also suggested that an inverse thermal flow (or apparent negative thermal conductivity) might be achieved by changing the geometrical shape of the shell[66]. These innovative theoretical concepts have been realized in experiments by constructing a thermal shield made of alternating concentric cylinders of latex rubber and a silicone elastomer, and placing the shield within an agar–water matrix (Fig. 7a)[69]. Under a thermal gradient, a constant temperature profile is obtained in the shield's inner region while the temperature profile outside is almost undistorted. On the other hand, by intentionally arranging the materials along the radial direction, the shell can act as a thermal concentrator, with the thermal energy considerably enhanced within the shell and remaining uniform (Fig. 7b). Even more surprisingly, for a spiral arrangement of the layers in the shell, heat rotates within the composite shell in a spiral manner such that heat flux (and the thermal gradient) changes its sign within the inner region of the shell—creating an apparent negative thermal conductivity (Fig. 7c)[69].

Thus heat management using metamaterials brings exciting new techniques with which to manipulate thermal energy. In analogy to optical and acoustical metamaterials, these offer unprecedented control of heat conduction.

Nanoscale heat transport and thermoelectrics

An additional important aspect of heat management is the need to reduce the amount of heat transport to ultralow levels. Materials with low thermal conductivities strongly affect the efficiency of thermoelectrics—which convert waste heat to electricity and provide an alternative source of energy for the future. In recent years, different strategies have been employed to enhance the efficiency of thermoelectrics, which is determined by the figure of merit $ZT = S^2\sigma T/\kappa$, where T is the temperature, S is the Seebeck coefficient, σ is the electrical conductivity and κ is the thermal conductivity. One approach involves the manipulation of the electronic properties—using quantum wells and wires—such that S and σ (and thus ZT) are increased[71]. Most recent efforts for enhanced thermoelectrics, however, have been based on reducing the thermal conductivity through nanostructuring. This has opened up promising opportunities to design and fabricate highly efficient thermoelectric materials. The remarkable progress in thermoelectrics is demonstrated by the large number of nanostructures with low thermal conductivities and enhanced thermoelectric efficiencies that have been fabricated[72–79].

Initial studies indicated that the Bi_2Te_3/Sb_2Te_3 and PbSe/PbTe quantum-dot superlattices exhibit enhanced thermoelectric properties[72,73]. Their high ZT values were attributed to the strong reduction in the thermal conductivity. Essentially, studies on superlattices demonstrate that the efficiency of thermoelectrics can be increased by purposely adding interfaces that act as scattering centres for phonons, reducing their mean free paths and therefore the thermal conductivity. In addition to atomic-layer-deposition structures, bulk thermoelectrics made of nanostructured AgPbSbTe compounds were shown to provide high ZT values[74]. In these materials, nanometre-scale quantum dots are produced through a thermal processing technique. In analogy to superlattices, the quantum-dot interfaces strongly scatter phonons, providing a mechanism for reducing the thermal conductivity and increasing the figure of merit ZT.

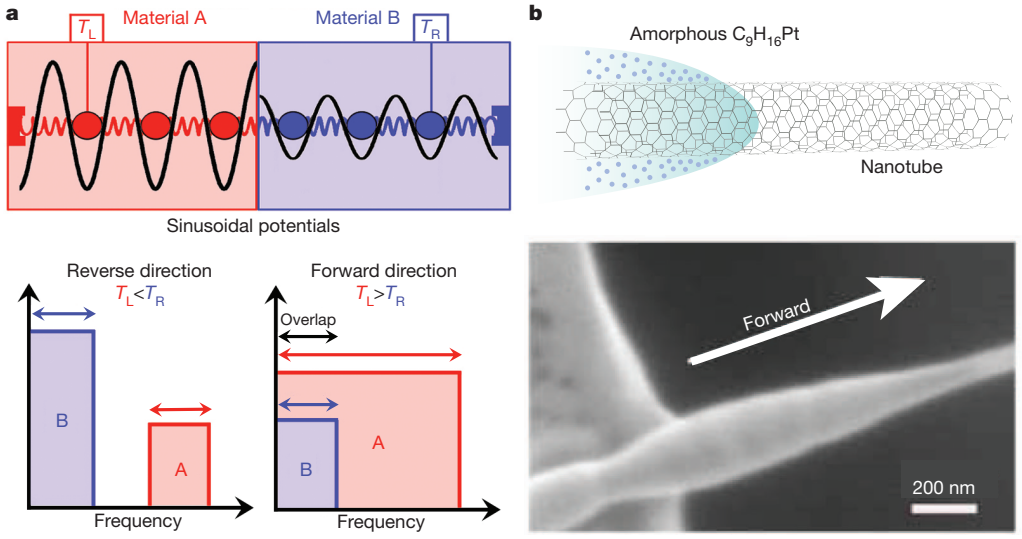

Figure 6 | Thermal diodes. a, Schematic of a thermal diode concept using two coupled nonlinear one-dimensional lattices. If $T_L < T_R$, (where 'L' means left and 'R' means right), vibrations in material B concentrate at low frequencies, but in material A they concentrate at high frequencies. The frequencies do not match, so heat cannot flow efficiently from right to left (reverse direction). If $T_L > T_R$, material A expands its vibrations to low frequencies, overlapping with those from material B, and heat is allowed to flow through the structure (forward direction). Adapted from ref. 63 with permission. **b**, Schematic and scanning electron microscope image of a boron nitride nanotube thermal diode with asymmetric deposition of amorphous $C_9H_{16}Pt$. For asymmetric nanotubes, higher thermal conductances are measured when heat flows from a high-mass region to a low-mass region. Reproduced from fig. 3b of ref. 64 with permission.

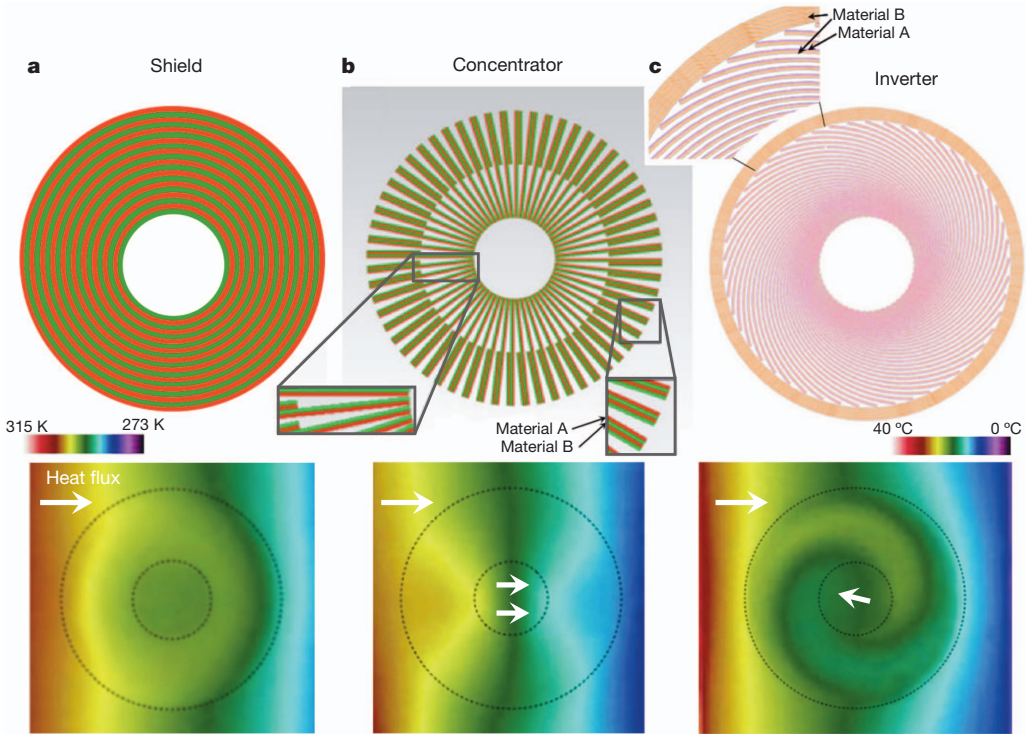

Figure 7 | Thermal metamaterials. **a**, A thermal shield made of a concentric layered structure of latex rubber and silicone elastomer (top). The measured temperature profile for horizontal heat flux (white arrow): the shell maintains the inner region at constant temperature (bottom). **b**, A thermal concentrator made of azimuthally alternating layers of latex and elastomer (top). The temperature profile, where heat flux is increased by 44% in the inner region (bottom). **c**, A thermal inverter made of a spiral arrangement of copper and polyurethane (top). The temperature profile showing inversion of the heat flux (bottom). Reproduced from figs 2, 3i, 4c and 6a of ref. 69 with permission.

Enhanced thermoelectric efficiencies by reducing heat transport can also be achieved by combining alloys and nanoparticles[75]. Thermal conductivity values below the alloy limit were obtained by epitaxially embedding ErAs nanoparticles in an $In_{0.53}Ga_{0.47}As$ alloy. The basic idea is that the alloy matrix scatters short-wavelength phonons and the ErAs nanoparticles stop mid-to-long-wavelength phonons, reducing the thermal conductivity below the alloy limit and improving thermoelectric efficiency. Another way of reducing phonon transport uses bulk nanocomposites made of BiSbTe alloys with nanosize grains[76]. In this 'polycrystal' technique, the material is converted into a nanoparticle dust by ball milling and then hot-pressed such that the nanoparticles merge together, creating nanosize grains. Measurements show[76] that the enhanced thermoelectric properties are the result of a significant reduction in thermal conductivity (the reduction is caused by scattering of phonons at the grain boundaries).

A significant reduction in thermal transport has also been achieved in silicon nanowires[77,78]. Large-area arrays of silicon nanowires grown by electrochemical synthesis show a surprising hundred-fold reduction in thermal conductivity[77]. The main reason for this reduction is the shortening of the phonons' mean free paths by phonon scattering at the rough nanowire surfaces. The development of theoretical models that can describe such ultralow thermal conductivities is currently an intense research area ranging from atomistic calculations to Boltzmann transport models.

More recently, the combination of various scattering processes has been employed to reduce heat transport greatly in PbTe-based thermoelectric materials[79]. First, atomic-scale substitutions (2 mol.% doping with Na) are introduced in a bulk PbTe sample to generate a figure of merit $ZT \approx 1.1$ at 775 K. By including endotaxial SrTe nanoparticles with 2–10 nm sizes, ZT is increased to about 1.7 at 800 K. Then, by transforming the sample to a polycrystal material with micrometre grain sizes, a ZT value of about 2.2 is achieved at 915 K (ref. 79). The nanocomposite provides a high ZT owing to the different length scales in the structure, which scatter phonons with different wavelengths. Essentially, atomic-scale substitutions block short-wavelength phonons, nanoparticles block mid-wavelength phonons and micrograins block large-wavelength phonons. These combined processes create an ultralow thermal conductivity and a highly efficient thermoelectric. The Na-doped PbTe–SrTe matrix was synthesized by melting and quenching, while the polycrystal was produced by powder processing and spark plasma sintering.

The idea of reducing heat transport through nanostructuring has been the basis for many recent advances in thermoelectric materials. The search for an easy-to-craft nanostructure with low thermal conductivity is now one of the main challenges in thermoelectrics. Equally importantly, nanostructured materials show us that interface scattering is a very effective mechanism of stopping the flow of phonons in the high-frequency (terahertz) part of the phononic spectrum[72–80].

Thermocrystals and coherent heat effects

An entirely new way of controlling heat transport, by which heat flow can be managed like sound waves[81], has recently been developed using 'thermocrystals', which are periodic structures made of alloys containing nanoparticles (Fig. 8a). The basic idea of thermocrystals is to manipulate the heat frequency spectrum such that low-frequency phonons carry a considerable part of the heat. In this manner, heat-carrying phonons are subject to coherent reflection and transmission at interfaces, and thus many applications designed for sound management can be applied to heat flow.

In thermocrystals[81], high-frequency phonons are blocked by including alloy atoms and nanoparticles ($d \approx 1$ nm). The alloy atoms scatter high-frequency phonons, while the nanoparticles block another set of high-frequency phonons[82–84]. In contrast to thermoelectrics[82], very high-frequency phonons are blocked in thermocrystals[81]. Because high-frequency phonons are severely restricted from carrying heat, the proportion of heat carried by low-frequency phonons increases (Fig. 8b). To concentrate heat around a specific frequency range—with the purpose of matching the PBG—the contribution of very low-frequency phonons is also reduced by considering a thin-film material with rough surfaces. As a result of blocking the highest and lowest frequencies, most heat is thus concentrated to a relatively narrow low-frequency band. Specifically, for a $Si_{90}Ge_{10}$ alloy with a 10% filling fraction of $d \approx 1$ nm Ge nanoparticles, the frequency band is $0.1\ \text{THz} < f < 2\ \text{THz}$, with up to 40% of the heat restricted to a narrow 'hypersonic' 100–300-GHz range (Fig. 8b). Taking advantage of this reduced heat spectrum, phononic crystals[12,85] with periodicities $a \approx 10$–20 nm are designed such that their PBGs match the frequencies of this narrow hypersonic range. These crystals are created by introducing air holes in the SiGe alloy thin film containing nanoparticles (Fig. 8a). In these 'thermocrystals' up to 23% of heat is carried by phonons with frequencies within the PBG.

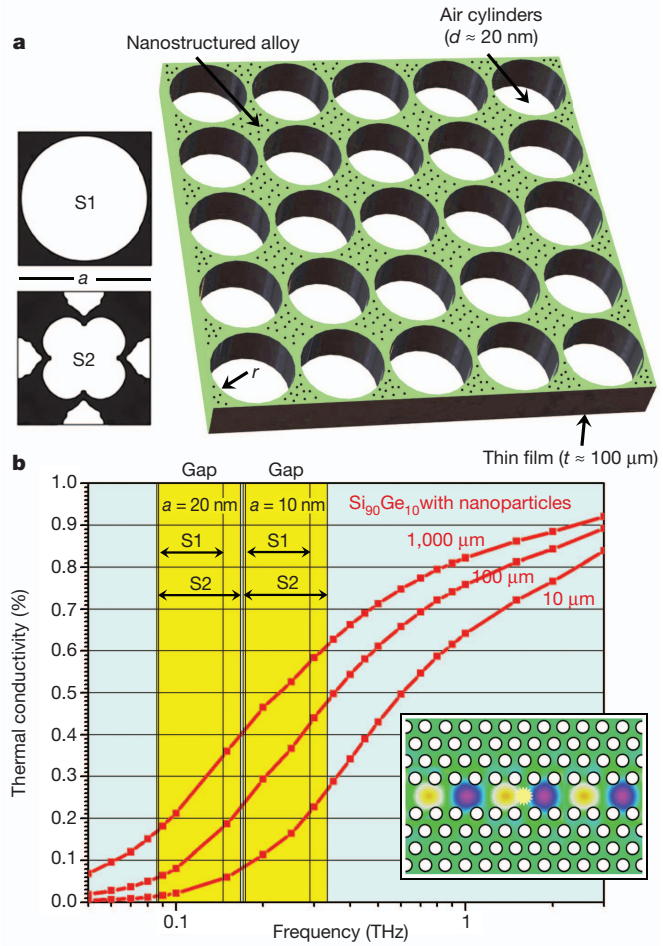

Figure 8 | Thermocrystals. **a**, Schematic of a thermocrystal made of air cylinders on a nanostructured alloy film[81]. **b**, Red shows the cumulative thermal conductivity as a function of frequency for $Si_{90}Ge_{10}$ nanoparticle films with different thicknesses. Yellow shows the frequency bandgaps for films patterned with a square arrangement of cylinders (S1) and with the design (S2). The inset shows that among the opportunities provided by thermocrystals is the possibility of guiding heat by removing a rod of cylinders. The colour scheme shows the displacement for a heat-carrying low-frequency phonon propagating within the waveguide.

This matching of the heat frequency spectrum and the PBG demonstrates that thermal phonons can be managed through coherent interference effects. In the past, phononic crystals have been shown to manage sound waves, but these are the first phononic crystals designed to control heat-carrying phonons. Thermocrystals lay the foundation for various applications such as heat waveguides, thermal lattices, heat imaging, thermo-optics, thermal diodes and thermal cloaking.

Conclusions and perspectives

Newly developed phononic crystals and metamaterials are both able to control phonon transport successfully at low and high frequencies in the phononic spectrum, ranging from sound to heat transfer. There is, however, an important difference between phonon management based on phononic crystals and that based on metamaterials. Whereas in phononic crystals the structure periodicity is generally of the same order as the wavelengths of the phonons to be controlled, in metamaterials the structure length scale can be smaller. This means that if we want to control large wavelengths in the phononic spectrum (Fig. 1), such as earthquake or tsunami waves, it would be more appropriate to use metamaterials, because the required periodicities for phononic crystals would be exceedingly large. On the other hand, if we want to manipulate the short-wavelength limit, that is, heat flow, then both thermocrystals and thermal metamaterials may be appropriate choices depending on the structure length scale and intended applications, because heat flow can be controlled by using millimetre-scale metamaterials or nanometre-scale thermocrystals.

I have also shown that heat flow can be blocked to ultralow levels using a large variety of nanostructured materials. This large reduction of the thermal conductivity is a consequence of diffuse interface scattering. When the nanostructured material is periodic, however, heat flow can be affected by two different physical mechanisms: diffuse interface scattering or coherent wave interference. For a periodic nanostructure to control heat coherently—and act as a phononic crystal—the wavelengths of heat-carrying phonons must be similar to the structure periodicity, $\lambda \approx 2a$ (Bragg reflection). Given that most heat phonon wavelengths in standard semiconductors at room temperature are relatively short ($\lambda \approx 1$–10 nm in silicon), the Bragg condition is essentially not satisfied in typical periodic nanostructures, and this prevents heat manipulation by PBGs. By increasing heat phonon wavelengths using thermocrystals, however, coherent wave-interference effects (and heat wave transport) can be achieved in nanostructures that are periodic.

This Review has shown that the development of new ideas for phonon management—combined with the ability to design and fabricate composite materials from the macroscale to the nanometre scale—has fuelled recent progress in sonic and thermal diodes, acoustic and thermal metamaterials, optomechanical crystals, hypersonic phononic crystals, thermoelectrics and thermocrystals. These advances have greatly increased our ability to manage the phononic spectrum at all relevant frequencies: sound, ultrasound, hypersound and heat. The emerging field of phonon management has great potential for innovations in materials and devices that can precisely manipulate sound and heat. Our ability to control electrons and photons has driven major technological revolutions in past decades; perhaps from our new ability to control phonons precisely we may expect analogously surprising and exciting consequences.

Received 19 April; accepted 28 August 2013.

1. Kushwaha, M. S., Halevi, P., Dobrzynski, L. & Djafari-Rouhani, B. Acoustic band structure of periodic elastic composites. *Phys. Rev. Lett.* **71,** 2022–2025 (1993).
2. Sigalas, M. M. & Economou, E. N. Band structure of elastic waves in two dimensional systems. *Solid State Commun.* **86,** 141–143 (1993).
3. Martínez-Sala, R. *et al.* Sound attenuation by sculpture. *Nature* **378,** 241 (1995).
4. Sanchez-Perez, J. V. *et al.* Sound attenuation by a two-dimensional array of rigid cylinders. *Phys. Rev. Lett.* **80,** 5325–5328 (1998).
5. Montero de Espinosa, F. R., Jimenez, E. & Torres, M. Ultrasonic band gap in a periodic two-dimensional composite. *Phys. Rev. Lett.* **80,** 1208–1211 (1998).
6. Liu, Z. Y. *et al.* Locally resonant sonic materials. *Science* **289,** 1734–1736 (2000).
7. Vasseur, J. O. *et al.* Experimental and theoretical evidence for the existence of absolute acoustic band gaps in two-dimensional solid phononic crystals. *Phys. Rev. Lett.* **86,** 3012–3015 (2001).
8. Gorishnyy, T., Ullal, C. K., Maldovan, M., Fytas, G. & Thomas, E. L. Hypersonic phononic crystals. *Phys. Rev. Lett.* **94,** 115501 (2005).
This paper describes the experimental realization of small-scale phononic crystals that control high-frequency hypersonic phonons.
9. Cheng, W., Wang, J., Jonas, U., Fytas, G. & Stefanou, N. Observation and tuning of hypersonic bandgaps in colloidal crystals. *Nature Mater.* **5,** 830–836 (2006).
10. Thomas, E. L., Gorishnyy, T. & Maldovan, M. Phononics: colloidal crystals go hypersonic. *Nature Mater.* **5,** 773–774 (2006).
11. Yu, J.-K., Mitrovic, S., Tham, D., Varghese, J. & Heath, J. R. Reduction of thermal conductivity in phononic nanomesh structure. *Nature Nanotechnol.* **5,** 718–721 (2010).
12. Maldovan, M. & Thomas, E. L. Simultaneous localization of phonons and photons in two-dimensional periodic structures. *Appl. Phys. Lett.* **88,** 251907 (2006).
13. Liang, B., Yuan, B. & Cheng, J. C. Acoustic diode: rectification of acoustic energy flux in one-dimensional systems. *Phys. Rev. Lett.* **103,** 104301 (2009).
14. Liang, B., Guo, X. S., Tu, J., Zhang, D. & Chen, J. C. An acoustic rectifier. *Nature Mater.* **9,** 989–992 (2010).
15. Li, B. Acoustics: now you hear me, now you don't. *Nature Mater.* **9,** 962–963 (2010).
16. Li, X.-F. *et al.* Tunable unidirectional sound propagation through a sonic-crystal-based acoustic diode. *Phys. Rev. Lett.* **106,** 084301 (2011).
This paper describes the experimetal realization of an acoustic diode by breaking spatial inversion symmetry in phononic crystals.
17. Boechler, N., Theocharis, G. & Daraio, C. Bifurcation-based acoustic switching and rectification. *Nature Mater.* **10,** 665–668 (2011).

18. Pendry, J. B., Schurig, D. & Smith, D. R. Controlling electromagnetic fields. *Science* **312,** 1780–1782 (2006).
19. Leonhardt, U. Optical conformal mapping. *Science* **312,** 1777–1780 (2006).
20. Milton, G. W., Briane, M. & Willis, J. R. On cloaking for elasticity and physical equations with a transformation invariant form. *New J. Phys.* **8,** 248 (2006).
21. Cummer, S. A. & Schurig, D. One path to acoustic cloaking. *New J. Phys.* **9,** 45 (2007).
22. Chen, H. & Chan, C. T. Acoustic cloaking in three dimensions using acoustic metamaterials. *Appl. Phys. Lett.* **91,** 183518 (2007).
23. Cummer, S. A. *et al.* Scattering theory derivation of a 3D acoustic cloaking shell. *Phys. Rev. Lett.* **100,** 024301 (2008).
24. Chen, H. & Chan, C. T. Acoustic cloaking and transformation acoustics. *J. Phys. D* **43,** 113001 (2010).
25. Torrent, D. & Dehesa-Sanchez, J. Acoustic cloaking in two-dimensions: a feasible approach. *New J. Phys.* **10,** 063015 (2008).
26. Cheng, Y., Yang, F., Xu, J. Y. & Liu, X. J. A multilayer structured acoustic cloak with homogeneous isotropic materials. *Appl. Phys. Lett.* **92,** 151913 (2008).
27. Zhang, S., Cia, X. & Fang, N. Broadband acoustic cloak for ultrasound waves. *Phys. Rev. Lett.* **106,** 024301 (2011).
This paper describes the experimental realization of acoustic cloaking shells for ultrasound waves using purpose-designed metamaterials.
28. Chan, C. T. Invisibility cloak for ultrasonic waves. *Physics* **4,** 2 (2011).
29. Farhat, M., Enoch, S., Guenneau, S. & Movchan, A. B. Broadband cylindrical acoustic cloak for linear surface waves in a fluid. *Phys. Rev. Lett.* **101,** 134501 (2008).
30. Popa, B. I., Zigoneanu, L. & Cummer, S. A. Experimental acoustic ground cloak in air. *Phys. Rev. Lett.* **106,** 253901 (2011).
31. Stenger, N., Wilhelm, M. & Wegener, M. Experiments on elastic cloaking in thin plates. *Phys. Rev. Lett.* **108,** 014301 (2012).
32. Farhat, M., Guenneau, S. & Enoch, S. Ultrabroadband elastic cloaking in thin plates. *Phys. Rev. Lett.* **103,** 024301 (2009).
33. Brun, M., Guenneau, S. & Movchan, A. B. Achieving control of in-plane elastic waves. *Appl. Phys. Lett.* **94,** 061903 (2009).
34. Trigo, M., Bruchhausen, A., Fainstein, A., Jusserand, B. & Thieryy-Mieg, V. Confinement of acoustical vibrations in semiconductor planar phonon cavity. *Phys. Rev. Lett.* **89,** 227402 (2002).
35. Worlock, J. M. & Roukes, M. L. Son et lumière. *Nature* **421,** 802–803 (2003).
36. Yablonovitch, E. Inhibited spontaneous emission in solid-state physics and electronics. *Phys. Rev. Lett.* **58,** 2059–2062 (1987).
37. John, S. Strong localization of photons in certain disordered dielectric superlattices. *Phys. Rev. Lett.* **58,** 2486–2489 (1987).
38. Joannopoulos, J. D., Villeneuve, P. R. & Fan, S. Photonic crystals: putting a new twist on light. *Nature* **386,** 143–149 (1997).
39. Maldovan, M. & Thomas, E. L. *Periodic Structures and Interference Lithography: for Photonics, Phononics and Mechanics* (Wiley, 2008).
40. Eichenfield, M., Chan, J., Camacho, R. M., Vahala, K. J. & Painter, O. Optomechanical crystals. *Nature* **462,** 78–82 (2009).
This paper describes the experimental demonstration of phonon–photon coupling in planar 'optomechanical' crystals.
41. Psarobas, I. E. *et al.* Enhanced acousto-optic interactions in a one-dimensional phoxonic cavity. *Phys. Rev. B* **82,** 174303 (2010).
42. Fainstein, A., Lanzillotti-Kimura, N. D., Jusserand, B. & Perrin, B. Strong optical-mechanical coupling in a vertical GaAs/AlAs microcavity for subterahertz phonons and near-infrared light. *Phys. Rev. Lett.* **110,** 037403 (2013).
43. Sadat-Saleh, S., Benchabane, S., Baida, F. I., Bernal, M. P. & Laude, V. Tailoring simultaneous photonic and phononic band gaps. *J. Appl. Phys.* **106,** 074912 (2009).
44. Mohammadi, S., Eftekhar, A. A., Khelif, A. & Adibi, A. Simultaneous two-dimensional phononic and photonic band gaps in opto-mechanical crystal slabs. *Opt. Express* **18,** 9164–9172 (2010).
45. Pennec, Y. *et al.* Simultaneous existence of phononic and photonic bandgaps in periodic crystal slabs. *Opt. Express* **18,** 14301–14310 (2010).
46. Safavi-Naeini, A. H. & Painter, O. Design of optomechanical cavities and waveguides on a simultaneous bandgap phononic-photonic crystal slab. *Opt. Express* **18,** 14926–14943 (2010).
47. Safavi-Naeini, A. H., Mayer Alegre, T. P., Winger, M. & Painter, O. Optomechanics in an ultrahigh-Q two-dimensional photonic crystal cavity. *Appl. Phys. Lett.* **97,** 181106 (2010).
48. Gavartin, E. *et al.* Optomechanical coupling in a two-dimensional photonic crystal defect cavity. *Phys. Rev. Lett.* **106,** 203902 (2011).
49. Chan, J. *et al.* Laser cooling of a nanomechanical oscillator into its quantum ground state. *Nature* **478,** 89–92 (2011).
50. Safavi-Naeini, A. H. *et al.* Observation of quantum motion of a nanomechanical resonator. *Phys. Rev. Lett.* **108,** 033602 (2012).
51. Safavi-Naeini, A. H. *et al.* Electromagnetically induced transparency and slow light with optomechanics. *Nature* **472,** 69–73 (2011).
52. Heinrich, G., Ludwig, M., Qian, J., Kubala, B. & Marquardt, F. Collective dynamics of optomechanical arrays. *Phys. Rev. Lett.* **107,** 043603 (2011).
53. Grudinin, I. S., Lee, H., Painter, O. & Vahala, K. J. Phonon laser action in a tunable two-level system. *Phys. Rev. Lett.* **104,** 083901 (2010).
54. Akimov, A. V. *et al.* Hypersonic modulation of light in three-dimensional photonic and phononic band gap materials. *Phys. Rev. Lett.* **101,** 033902 (2008).
55. Papanikolaou, N., Psarobas, I. E. & Stefanou, N. Absolute spectral gaps for infrared light and hypersound in three-dimensional metallodielectric phoxonic crystals. *Appl. Phys. Lett.* **96,** 231917 (2010).
56. Russell, P. S. J., Marin, E., Diez, A., Guenneau, S. & Movchan, A. B. Sonic band gaps in PCF preforms: enhancing the interaction of sound and light. *Opt. Express* **11,** 2555–2560 (2003).
57. Laude, V. *et al.* Phononic bandgap guidance of acoustic modes in photonic crystal fibers. *Phys. Rev. B* **71,** 045107 (2005).
58. Dainese, P. *et al.* Stimulated Brillouin scattering from multi-GHz-guided acoustic phonons in nanostructured photonic crystal fibres. *Nature Phys.* **2,** 388–392 (2006).
59. Kang, M. S., Nazarkin, A., Brenn, A. & Russell, P. S. J. Tightly trapped acoustic phonons in photonic crystal fibres as highly nonlinear artificial Raman oscillators. *Nature Phys.* **5,** 276–280 (2009).
60. Li, B. W., Wang, L. & Casati, G. Thermal diode: rectification of heat flux. *Phys. Rev. Lett.* **93,** 184301 (2004).
61. Terraneo, M., Peyrard, M. & Casati, G. Controlling the energy flow in nonlinear lattices: a model for a thermal rectifier. *Phys. Rev. Lett.* **88,** 094302 (2002).
62. Wang, L. & Li, B. Thermal logic gates: computation with phonons. *Phys. Rev. Lett.* **99,** 177208 (2007).
63. Wang, L. & Li, B. Phononics get hot. *Phys. World* **21,** 27–29 (2008).
64. Chang, C. W., Okawa, D., Majumdar, A. & Zettl, A. Solid-state thermal rectifier. *Science* **314,** 1121–1124 (2006).
This paper describes an experimental solid-state thermal diode formed by a non-uniform mass distribution in nanotubes.
65. Yang, N., Li, N., Wang, L. & Li, B. Thermal rectification and negative differential thermal resistance in lattices with mass gradient. *Phys. Rev. B* **76,** 020301 (2007).
66. Fan, C. Z., Gao, Y. & Huang, J. P. Shaped graded materials with an apparent negative thermal conductivity. *Appl. Phys. Lett.* **92,** 251907 (2008).
67. Chen, T., Weng, C. N. & Chen, J. S. Cloak for curvilinearly anisotropic media in conduction. *Appl. Phys. Lett.* **93,** 114103 (2008).
68. Guenneau, S., Amra, C. & Veynante, D. Transformation thermodynamics: cloaking and concentrating heat flux. *Opt. Express* **20,** 8207–8218 (2012).
69. Narayana, S. & Sato, Y. Heat flux manipulation by engineered thermal materials. *Phys. Rev. Lett.* **108,** 214303 (2012).
This paper describes the manipulation of heat conduction using newly developed thermal metamaterials.
70. Schittny, R., Kadic, M., Guenneau, S. & Wegener, M. Experiments on transformation thermodynamics: molding the flow of heat. *Phys. Rev. Lett.* **110,** 195901 (2013).
71. Hicks, L. D. & Dresselhaus, M. S. Effect of quantum-well structures on the thermoelectric figure of merit. *Phys. Rev. B* **47,** 12727–12731 (1993).
72. Venkatasubramanian, R., Siivola, E., Colpitts, T. & O'Quinn, B. Thin-film thermoelectric devices with high-room temperature figures of merit. *Nature* **413,** 597–602 (2001).
73. Harman, T. C., Taylor, P. J., Walsh, M. P. & LaForge, B. E. Quantum dot superlattice thermoelectric materials and devices. *Science* **297,** 2229–2232 (2002).
74. Hsu, K. F. *et al.* Cubic $AgPb_mSbTe_{2+m}$: bulk thermoelectric materials with high figure of merit. *Science* **303,** 818–821 (2004).
75. Kim, W. *et al.* Thermal conductivity reduction and thermoelectric figure of merit increase by embedding nanoparticles in crystalline semiconductors. *Phys. Rev. Lett.* **96,** 045901 (2006).
76. Poudel, B. *et al.* High-thermoelectric performance of nanostructured bismuth antimony telluride bulk alloys. *Science* **320,** 634–638 (2008).
77. Hochbaum, A. I. *et al.* Enhanced thermoelectric performance of rough silicon nanowires. *Nature* **451,** 163–167 (2008).
78. Boukai, A. I. *et al.* Silicon nanowires as efficient thermoelectric materials. *Nature* **451,** 168–171 (2008).
79. Biswas, K. *et al.* High-performance bulk thermoelectrics with all-scale hierarchical structures. *Nature* **489,** 414–418 (2012).
This paper describes a highly efficient thermoelectric material obtained through the scattering of a wide range of phonons with different wavelengths.
80. Chiritescu, C. *et al.* Ultra low thermal conductivity in disordered WSe_2 crystals. *Science* **315,** 351–353 (2007).
81. Maldovan, M. Narrow low-frequency spectrum and heat management by thermocrystals. *Phys. Rev. Lett.* **110,** 025902 (2013).
82. Mingo, N., Hauser, D., Kobayashi, N. P., Plissonnier, M. & Shakouri, A. Nanoparticle in alloy approach to efficient thermoelectrics: silicides in SiGe. *Nano Lett.* **9,** 711–715 (2009).
83. Garg, J., Bonini, N., Kozinsky, B. & Marzari, N. Role of disorder and anharmonicity in the thermal conductivity of silicon germanium alloys: a first principle study. *Phys. Rev. Lett.* **106,** 045901 (2011).
84. Kundu, A., Mingo, N., Broido, D. A. & Stewart, D. A. Role of light and heavy embedded nanoparticles on the thermal conductivity of SiGe alloys. *Phys. Rev. B* **84,** 125426 (2011).
85. Bilal, O. R. & Hussein, M. I. Ultrawide phononic band gap for combined in-plane and out-of-plane waves. *Phys. Rev. E* **84,** 065701 (2011).

Author Information Reprints and permissions information is available at www.nature.com/reprints. The author declares no competing financial interests. Readers are welcome to comment on the online version of the paper. Correspondence and requests for materials should be addressed to M.M. (maldovan@gatech.edu).